Chinese Chemical Letters 35 (2024) 108442

Contents lists available at ScienceDirect

Chinese Chemical Letters

journal homepage: www.elsevier.com/locate/cclet

New insight into polystyrene ion exchange resin for efficient cesium sequestration: The synergistic role of confined zirconium phosphate nanocrystalline

Mengzhou Wang[a], Mingyan Fu[a], Junfeng Li[b], Yihui Niu[a], Qingrui Zhang[a,*], Qina Sun[a,*]

[a] Hebei Key Laboratory of Heavy Metal Deep-Remediation in Water and Resource Reuse, School of Environmental and Chemical Engineering, Yanshan University, Qinhuangdao 066004, China
[b] Laboratory of Environmental Technology, INET, Tsinghua University, Beijing 100084, China

ARTICLE INFO

Article history:
Received 20 December 2022
Revised 20 March 2023
Accepted 10 April 2023
Available online 11 April 2023

Keywords:
Zirconium phosphate
Nanocrystalline
Polystyrene resin
Cesium
Removal

ABSTRACT

Polystyrene resins (PS) have been practical ion exchangers for radionuclides removal from water. However, nonspecific effects of ion exchange groups continue to be a major obstacle for emergency treatment with coexisting ions of high concentrations. The selectivity for Cs^+ enables zirconium phosphate (ZrP) to be the most promising inorganic sorbent for radioactive cesium extraction, despite being difficult to synthesize and causing excessive pressure loss in fixed-bed reactors due to fine powder. Herein, through facile confined crystallization in host macropores, we prepared PS confined α-ZrP nanocrystalline (ZrP-PS). Size-screen sorption of layered α-ZrP and sulfonic acid group preconcentration of PS synergistically enable a considerably higher Cs^+ affinity of ZrP-PS than PS, as confirmed by X-ray photoelectron spectroscopy (XPS) analysis. ZrP-PS demonstrated remarkable cesium sequestration performance in both batch and continuous experiments, with a high adsorption capacity of 269.58 mg/g, a rapid equilibrium within 80 min, and a continuous effluent volume of 2300 L/kg sorbents. Given the excellent selectivity for Cs^+ and flexibility to separate from treated water, ZrP-PS holds great promise as purification packages for the emergency treatment of radioactively contaminated water.

In the last 50 years, severe nuclear reactor accidents in Europe, Asia, and North America have caused local radiation to rise above natural background levels in the short term, as well as chronic contamination exceeding prescribed standards in different parts of the world [1–3]. The total discharges of radioactive cesium (mostly ^{137}Cs and ^{134}Cs) after the Fukushima accident were estimated at 27.1 PBq, the most massive amount of artificial radioactive material ever released into the sea [4]. As an alkali metal, radioactive cesium exists mainly as the cation of Cs^+ in water, migrates easily and eventually enters the human body through the food chain, increasing the risk of developing tumors through external and internal exposure [5–7]. Therefore, it is of imperative interests to sequestrate cesium from aqueous environments in nuclear emergency treatment.

Many separation technologies have been used to remove radioisotopes from wastewater in nuclear power plants, including Cs^+, such as precipitation, solvent extraction, evaporation concentration, membrane and ion exchange [8–10]. Ion exchange technology benefits from flexible operations, adaptability to various scenarios, easy integration of devices and recycling, especially from reducing the amount of final solid waste generated effectively by avoiding large amounts of radioactive sludge or organic solvents [11]. However, studies are inadequate on removing radioactive alkaline and alkaline earth metal cations by ion exchange resins when coexisting with cations of high concentration [12,13]. As a common feature of ionic pollutants purification by ion exchange resins, the nonspecific effect between ion exchange groups and ions may cause the competitive exchange of coexisting cations and reduce Cs^+ removal efficiency [14–17]. This low Cs^+ selectivity is the main limitation of ion exchange technology for emergency treatment in real waters.

Unlike ion exchange resins, inorganic ion exchangers such as zirconium compounds, metal hexacyanoferrates (MHCF), ammonium molybdophosphate (AMP), and clay minerals allow selective enrichment of alkaline metals and alkaline earth metals cations and halide anions [14,18–27]. For sequestrating cesium, the performances of Prussian blue, zeolite, and AMP still need to be improved regarding adsorption equilibrium time, adsorp-

* Corresponding authors.
E-mail addresses: zhangqr@ysu.edu.cn (Q. Zhang), sunqn@ysu.edu.cn (Q. Sun).

https://doi.org/10.1016/j.cclet.2023.108442
1001-8417/

tion capacity, and stability [14,18]. At the same time, zirconium phosphate (ZrP) has received much interest in recent decades on its excellent performance [23–27]. Since Clearfield and Alberti pioneered the synthesis and structural description of layered ZrP, analogous layered semicrystalline phosphates have been actively researched for solid acid catalysis, adsorption and drug delivery basing on their similar layered structures [23,24]. These semicrystalline ZrP are cationic layered compounds with a permanent surface charge and flexible layered structures bound by van der Waals forces, in which the Zr atoms connected *via* the HPO_4^{2-} groups with the pristine exchangeable counter-ions located within the interlayer space [25]. For the separation and extraction of fission products from high-level liquid wastes (HLLWs), ZrP and its derivatives exhibited remarkable Cs selectivity, very sparing aqueous solubility, and excellent radiation resistance, making them the most promising inorganic ion exchangers in Cs extraction [26]. However, it is still a problem for ZrP to be directly employed in flow-through treatment systems due to the excessive pressure drop from the fine powder, which greatly limits the practical engineering application of ZrP as the Cs-selective ion exchangers.

Despite its low selectivity of Cs^+, commercial resins have been proposed to be an ideal host for incorporating inorganic particles as an engineering application solution, notably polystyrene ion change resins (PS). In previous studies, PS-hosted nanoparticles were proved efficient in purifying trace heavy metal cations, oxyanions, and halide anions [28–31]. PS host primarily provides three benefits. Firstly, immobilize charged groups of the polymeric PS, namely the sulfonic acid group or quaternary ammonium group, permeate and preconcentration target ions by 'Donnan membrane effect' before surface bonding, enhancing final capacity of target ions [32]. Secondly, charged groups facilitate dispersion of small-size particles, providing greater adsorption capacities and/or faster adsorption rates [33]. Thirdly, millimeter-scale PS beads are appropriate for continuous flow systems for satisfactory hydrodynamic performance in typical water purification units like continuous packed columns. Thus, we speculate that PS-hosted ZrP exhibits efficient cesium sequestration and is feasible for continuous packed columns. Moreover, universal purification components for emergency treatment could be fabricated based on cesium sequestration behavior and mechanism by PS-hosted ZrP from complex aqueous environments. However, to the best of our knowledge, such research has not been reported.

Herein, we aim to sequestrate cesium using PS-hosted ZrP and investigate the behavior and mechanism of cesium sequestration. Through facile confined crystallization in the host macropores, we prepared the PS-confined α-ZrP nanocrystalline, noted as ZrP-PS. Batch sorption runs were performed to examine the adsorption performance of ZrP-PS on simulated radioactive cesium, including the effects of solution pH, coexisting ions, reaction temperature and time. A series of characterizations revealed the mechanism of cesium sequestration. By *in-situ* crystalline growth in macropores, nano α-ZrP was embedded in the porous inner surface of PS. The specific affinity between layered α-ZrP nanocrystalline and Cs^+ synergized the Donnan film effect of PS, which allowed cesium to be efficiently separated from water coexisting with high-concentration cations. The continuous packed column assessment predicted ZrP-PS to be an excellent solution for cesium sequestration in emergency treatment applications.

A polystyrene macroporous cation exchange resin charged with sulfonic acid groups ($-SO_3^-$) was used as host. Detailed materials, synthesis and characterization of ZrP-PS and Cs^+ adsorption experiment sections were in Support Information (Texts S1-S5 in Supporting information).

By a facile process similar to amorphous ZrP synthesis, nanocrystalline α-ZrP was dispersed in PS and confined in macropores of the host. ZrP-PS was shown with uniformly distributed

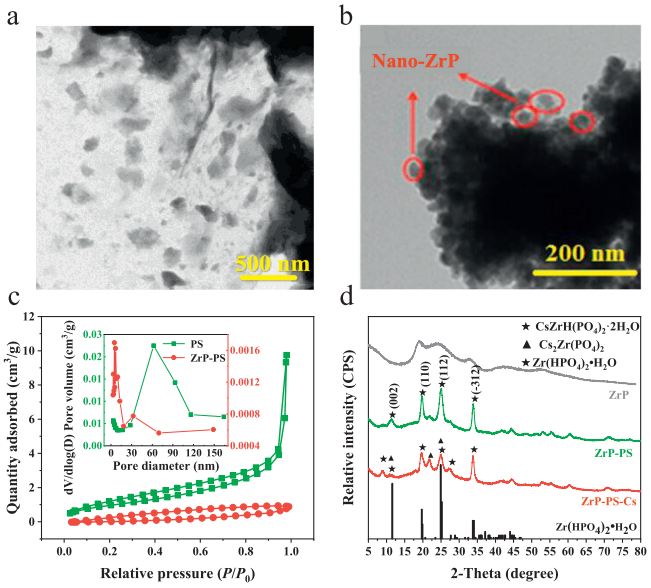

Fig. 1. Characterization of ZrP-PS and ZrP: (a) the TEM image of ZrP-PS and (b) the TEM images of ZrP powder, (c) nitrogen adsorption-desorption isotherms (inset: pore size distribution) of PS and ZrP-PS, and (d) XRD patterns of ZrP powder, ZrP-PS and Cs-sequestrated ZrP-PS (ZrP-PS-Cs), and the standard pattern of Zr(HPO4)2·H2O (top to bottom).

ZrP particles of diameters of 200–400 nm without aggregation (Fig. 1a). In contrast, nano ZrP synthesized without PS host aggregated severely only showing ~50 nm particles at the edges (Fig. 1b). For the N_2 sorption isotherms (Fig. 1c), macropores in PS exhibited a type II isotherm with a steep increase in adsorption volume at $P/P_0 = 0.95–1.00$, while the hysteresis loop of ZrP-PS appeared in the lower relative pressure range reflecting the decreased pore size distribution [34]. Also, the pore volume and average pore size of ZrP-PS both decreased (Fig. 1c, insert). The atomic force microscope (AFM) 3D analysis in Fig. S1a (Supporting information) showed that the vertical height approximate 200 nm of the central cross-section of ZrP-PS was smoother than that of PS. Both the N_2 sorption isotherms and the AFM images indicated pore confined ZrP blocked some macropores. Pore-confinement is also demonstrated by the gradually growth of ZrP from the outer surface to the inner part of PS (Text S6 and Fig. S1b in Supporting information). The confined ZrP exhibits the characteristic diffraction peaks at 2θ of 11.6, 20.3, and 24.9° in the X-ray powder diffractometer (XRD) pattern (Fig. 1d), which correspond to the crystal planes (002), (110), and (112) of crystalline α-$Zr(HPO_4)_2{\cdot}H_2O$ (α-ZrP, JCPDS No. 22–1022). The (002) crystal plane spacing was 7.6 Å calculated from Bragg's law (Text S7 in Supporting information), indicating the PS-confined ZrP was layered α-ZrP crystalline [35–38].

The typical synthesis of layered structural ZrP involves high-temperature calcination [24,38–40]. In this study, Zr^{4+}, as the ZrP precursor, dispersed throughout macropores of the PS host due to negative charges of $-SO_3^-$, which significantly altered the crystallization behavior of ZrP. Confined formation of the crystalline phase is possible because of altered crystallization kinetics and thermodynamics in PS pores [30,41]. Without pore-confinement, ZrP was mainly amorphous and showed broad diffraction peaks in XRD pattern (Fig. 1d). Accordingly, through porous and cross-linking matrix and ample surface charge of PS, α-ZrP was confined in the host, which was presumed to facilitate good cesium sequestration in addition to $-SO_3^-$ groups.

Cesium sequestration of ZrP-PS demonstrated removal efficiencies higher than 95.2% in the wide pH range of 3.27–10.93 (Fig. 2a). This performance benefited from the stably negative zeta poten-

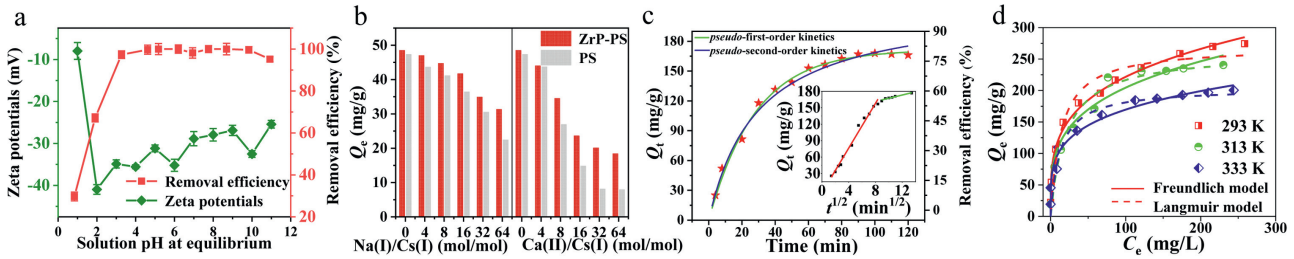

Fig. 2. (a) Solution pH effects on Cs^+ removal (ZrP-PS dose: 1.0 g/L, initial $Cs^+ = 50$ mg/L, 298 K for 24 h) and zeta potentials of ZrP-PS, (b) effects of competing cations Na^+ and Ca^{2+} on Cs^+ removal (sorbent dose 1.0 g/L, initial $Cs^+ = 50$ mg/L, 298 K for 24 h, pH 6.5–7.0), (c) kinetic models fitting results, inset: intraparticle diffusion model fitting (ZrP-PS dose: 0.4 g/L, initial $Cs^+ = 80$ mg/L, 298 K, pH 6.5–7.0), and (d) adsorption isotherm curves fitted by Langmuir and Freundlich models (ZrP-PS dose: 1.0 g/L, 24 h, pH 6.5–7.0).

tials of ZrP-PS due to permanently negatively charged -SO_3^- in PS [42]. H^+ release was observed in cesium sequestration by ZrP-PS (Fig. S2 in Supporting information), suggesting similar proton-Cs^+ exchange to that of amorphous ZrP, and thus an excess of H^+ ions inhibited the Cs^+ removal at pH values 0.84 and 1.91. Furthermore, surface protonation of ZrP-PS at high acidity resulted in the most positive zeta potential at pH around 1.0, which weakened nonspecific electrostatic interaction of ZrP-PS toward Cs^+, thereby affecting cesium sequestration.

It is essential for emergency treatment to investigate the selectivity of Cs^+ under coexistence of competing cations. Both ZrP-PS and PS were affected to some extent with increasing concentrations of Na^+ and Ca^{2+} (Fig. 2b). When Na^+/Cs^+ (mol/mol) was increased from 0 to 16, the Cs^+ removal efficiency by ZrP-PS remained greater than 90.0%; in contrast, that by PS decreased dramatically from 94.6% to 72.8% and was only 44.8% at Na^+/Cs^+ (mol/mol) = 64. When Ca^{2+}/Cs^+ (mol/mol) was increased from 0 to 32, the removal efficiency of Cs^+ by ZrP-PS decreased from 97.0% to 40.2%, while that of PS from 94.6% to 16.2%. However, with the further increase of Ca^{2+}/Cs^+, the removal efficiency of ZrP-PS stabilized. The solid-liquid distribution ratio K_d of ZrP-PS (310 mL/g) was about 24 times greater than that of PS (Text S8 in Supporting information). ZrP-PS is expected to sequestrate Cs^+ *via* proton exchange by ZrP [43] in addition to the nonspecific interaction of -SO_3^- groups, with the latter to be a main interaction of PS. The proton-exchange sites on α-ZrP provide a specific affinity and high selectivity for Cs^+, while the selectivity by PS with coexisting cations was inferior because cations competed the nonspecific sites of -SO_3^-. In addition, effects of Mg^{2+}, typical coexisting anions (Cl^-, NO_3^-, SO_4^{2-}), humic acid and salinity on Cs^+ selectivity supported the benefits of ZrP-PS for emergency treatment in natural waters (Text S9, Fig. S3 in Supporting information).

The adsorption kinetics and isotherm experiments were conducted through batch adsorption tests to investigate further the cesium sequestration performance of ZrP-PS (Text S10 in Supporting information). Fig. 2c shows the adsorption kinetics of Cs^+ on ZrP-PS, with PS as the reference in Fig. S4a (Supporting information). Cs^+ uptake equilibriums reached within ~80 min for both ZrP-PS and PS; however, ZrP-PS exhibited a faster kinetic process. Cs^+ removal efficiencies by ZrP-PS at 30 and 80 min were 55.1% and 84.5%, respectively. The *pseudo*-first-order, *pseudo*-second-order, and intraparticle diffusion models fitted the kinetic data of ZrP-PS well, with higher rate constants K_1, K_2 and K_{int} representing the faster kinetic rate than PS (Table S1 in Supporting information). The intraparticle diffusion model exhibited a higher correlation to ZrP-PS ($R^2 = 0.9825$) than PS ($R^2 = 0.8393$), inferring that decreased average pore size in ZrP-PS affected intraparticle diffusion of Cs^+. The isothermal adsorption data of Cs^+ on PS and ZrP-PS were fitted well by Langmuir and Freundlich models (Fig. 2d, Fig. S4b and Table S2 in Supporting information). According to the Langmuir model, the adsorption capacity of Cs^+ on PS was 230.61 mg/g and did not change much at the experimental temperatures. The adsorption capacity of Cs^+ by ZrP-PS increased with decreasing temperatures, indicating the exothermic nature of cation exchange of α-ZrP [44]. The maximum adsorption capacity of Cs^+ on ZrP-PS was 269.85 mg/g at 293 K, greater than that on PS and an almost unmatched maximum capacity for Cs^+ adsorption compared with the literature in the last ten years [45–54] (Table 1). In addition, when ZrP-PS was used in simulated radioactive wastewater (Table S3 in Supporting information), removal efficiency was not significantly influenced by high Cs^+ concentrations of 50 and 200 mg/L (Fig. S5 in Supporting information), further demonstrating efficient cesium sequestration performance of ZrP-PS.

To disclose the mechanism of efficient Cs^+ sequestration by ZrP-PS, XRD, Fourier transform infrared (FT-IR) spectra and X-ray photoelectron spectroscopy (XPS) analysis of different samples was performed, and the results are depicted in Figs. 1d and 3, Figs. S6 and S7 (Supporting information). By XPS analysis, differences of P 2p, Zr 3d and O 1s binding energies between PS-confined α-ZrP nanocrystalline and amorphous ZrP further approved the structural characteristics ZrP-PS and ZrP shown in the XRD patterns (Text S11 in Supporting information). After Cs^+ adsorption on ZrP-PS, cesium was detected in the ZrP-PS-Cs sample both in the XRD and XPS analyses, as the characteristic peaks of Cs^+ solid solutions ($Cs_2Zr(PO_4)_2$ and $CsZrH(PO_4)_2{\cdot}xH_2O$) in Fig. 1d and Cs 3d bonding energies at 725.0–740.0 eV in the full XPS spectrum shown in Fig. 3b. XRD characteristic peaks of α-ZrP were observed without position variation. FT-IR spectra comparison of ZrP-PS and ZrP-PS-Cs in Fig. 3a presents that most functional groups remained before and after Cs^+ adsorption, confirming the stable chemical composite of ZrP-PS. Weak bands at 1410 cm^{-1} of ZrP-PS are attributed to the presence of δ(POH), indicating the existence of structural hydroxyl as exchangeable proton sites in confined α-ZrP. This involvement of proton exchange in phosphate groups during Cs^+ adsorption could also be inferred from the notable reduction of the (002) peak intensity of ZrP-PS in Fig. 1d and the intensity changes of bands at 1035 and 670 cm^{-1} in Fig. S6 (Text S12 in Supporting information). More information on the mechanism of Cs^+ sequestration is revealed in the XPS spectra. In the high-resolution analysis, Cs $3d_{5/2}$ binding energy of ZrP-PS-Cs shifted 0.4 eV compared to the standard peak of $CsNO_3$ located at 724.2 eV (Fig. 3c) [55], and P 2p binding energy shifted from 134.2 eV of ZrP-Cs to 133.8 eV of ZrP-PS-Cs (Fig. S7d in Supporting information). These bonding energies shifts hint the strong interaction between Cs^+ and ZrP-PS. In addition, as shown in Fig. S7e (Supporting information), the Cs $3d_{5/2}$ peak around 723.8 eV is attributable to the electrostatic interaction of -SO_3^- toward Cs^+ (noted as -$SO_3^-Cs^+$), whereas the one around 724.1 eV is attributable to the ion exchange between Cs^+ and protons of P-O-H in α-ZrP (noted as P-O-Cs) [56]. The O 1s of ZrP-PS-Cs shows a broad peak which could correspond to O atoms bonded to Cs atoms in addition to those in Zr-O, P-O and

Table 1
Comparison of Cs adsorption capacities and kinetics by adsorbents in literatures in the last ten years.

Adsorbent	Capacity (mg/g)	Kinetics (min)	Year	Ref.
ZrP-PS	269.58	80	2022	This study
Potassium-directed layered metal sulfide $KInSnS_4$	281	180	2022	[45]
Granular activated carbon-covalent organic polymer-Prussian blue	1.091	120	2021	[46]
Fe_3O_4-chitosan-NaCuHCFe nanoparticles	161.3	200	2020	[47]
Ammonium molybdophosphate/polyvinyl alcohol/sodium alginate composite hydrogel	71.28	720	2019	[48]
Sulfur hosting mordenite	196	180	2018	[49]
Phosphomolybdic acid zirconium loaded on silocone	43.48	150	2017	[50]
Ammonium molybdophosphate loaded on silica matrix (20 wt% AMP)	15.48 ± 0.61	40	2016	[51]
Maghemite polyvinyl alcohol alginate beads	32.15	300	2015	[52]
Magnetic Prussian blue/graphene oxide	55.56	720	2014	[53]
Nickel hexacyanoferrate-walnut shell	4.94	120	2013	[54]

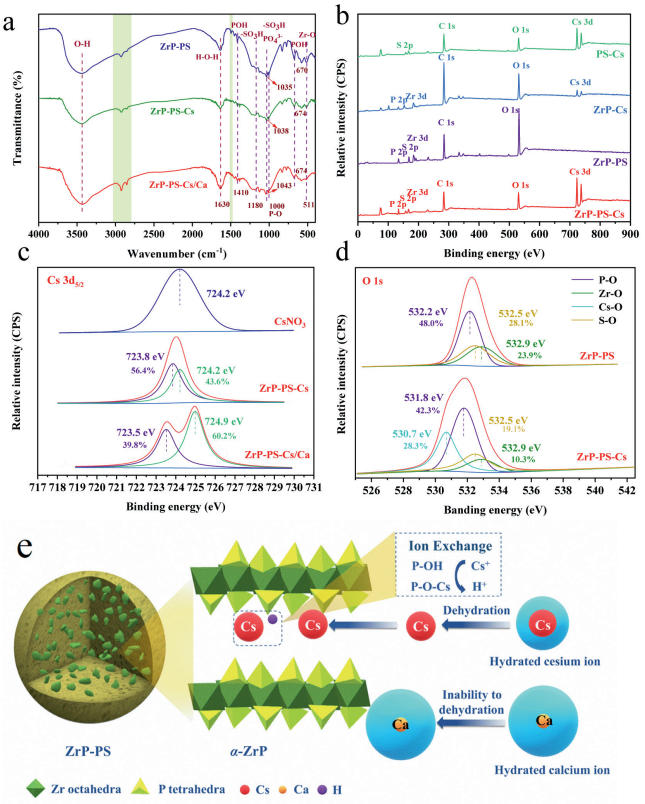

Fig. 3. (a) FT-IR spectra of ZrP-PS, ZrP-PS-Cs and ZrP-PS-Cs/Ca samples, (b) XPS survey spectra of PS-Cs, ZrP-Cs, ZrP-PS, and ZrP-PS-Cs, (c) Cs 3d5/2 XPS spectra of CsNO3, ZrP-PS-Cs, and ZrP-PS-Cs/Ca (Ca:Cs = 1) samples, (d) O 1s XPS spectra of Zr-PS and ZrP-PS-Cs, and (e) the illustration of synergistic role of confined α-ZrP on cesium sequestration.

S-O (Fig. 3d). The shift of O 1s from 532.2 eV to 531.8 eV after Cs^+ adsorption also suggests an interaction between Cs^+ and ZrP-PS using oxygen atoms as bridges, forming the P-O-Cs and lowering the O 1s binding energy [57]. Thus, proton exchange by P-OH and electrostatic interaction by $-SO_3H$ are associated mechanisms of Cs sequestration by ZrP-PS.

Furthermore, the synergy of α-ZrP is emphasized by characterizing the competing adsorption of Ca^{2+} on different materials. When Cs^+ and Ca^{2+} co-existed, the FT-IR peak of $-SO_3H$ at 1035 cm^{-1} blue-shifted by 6.75 cm^{-1}, more than just 1.84 cm^{-1} without Ca^{2+}, suggesting nonspecific interaction of $-SO_3H$ with both cations. Compared to fresh ZrP-PS, the POH peaks blue-shifted for 4 cm^{-1} after Cs sequestration without and with Ca^{2+} competitive adsorption, which implies specific interaction of P-O-H and Cs^+. In high-resolution XPS analysis of Cs $3d_{5/2}$ in Fig. S7e and Fig. 3c, negligible shift on Cs $3d_{5/2}$ binding energy could be observed from PS-Cs to ZrP-PS-Cs, but a –0.7 eV positive shift exhibited for ZrP-PS-Cs/Ca compared to PS-Cs. This is because of different deconvoluted peaks area portions with and without Ca^{2+} coexistence. In both cases, the Cs $3d_{5/2}$ spectra were divided into two peaks corresponding to P-O-Cs and $-SO_3^-Cs^+$. The area fractions of P-O-Cs and $-SO_3^-Cs^+$ of ZrP-PS-Cs were 18.2% and 81.8%, respectively. However, as for ZrP-PS-Cs/Ca, peak fractions varied distinguishably with 60.2% P-O-Cs and 39.8% $-SO_3^-Cs^+$. Such results certify that with high concentration Ca^{2+} coexistence, Cs sequestration by $-SO_3^-Cs^+$ path abated while P-O-Cs dominated and contributed high selectivity of Cs^+ by ZrP-PS.

Based on the removal performance and characteristic results, the mechanism of efficient Cs^+ sequestration by ZrP-PS was elucidated, as illustrated in Fig. 3e. Cs^+ sequestration by ZrP-PS is attributed to the synergistic effect of confined nanocrystalline α-ZrP and $-SO_3^-$ groups covalently binding in the PS polymer host.

Firstly, negatively charged $-SO_3^-$ groups enrich Cs^+ *via* electrostatic interaction, a fundamental effect of cation exchange resins, to a concentration higher than in the bulk solution by the Donnan membrane effect. This widely verified effect [28–32,34] promotes Cs^+ diffusion to interaction sites. Secondly, confined α-ZrP absorb Cs^+ through interlayer proton exchange. In α-ZrP, Zr atoms planes severe as the basic layered structure, with $-HPO_4$ groups attached by three O atoms coordinating to Zr. While the fourth O of $-HPO_4$, bearing a proton, points toward the interlayer space as a potential cation exchange site [37]. The maximum opening to the interlayer space expands to adequate for Cs^+ (radius 1.69 Å) to diffuse into interlayers and exchange with the proton in P-O-H [26,58-60], then the accessibility of Cs is constrained by crystal lattice match and restraint, shown as Eq. 1.

$$mCs^+\ (aq) + Zr(HPO_4)_2{\cdot}H_2O\ (s) + (x\text{-}1)H_2O \rightarrow Cs_mH_nZr(PO_4)_2{\cdot}xH_2O\ (s) + mH^+\ (aq)\ (m+n=2) \quad (1)$$

Thirdly, with the presence of monovalent alkali metal and divalent alkali earth metal cations that lacking outermost electron distinction from Cs^+, confined α-ZrP plays a vital role in selective adsorption toward Cs^+. Competitive Na/Ca/Mg cations occupied the nonspecific adsorption sites of $-SO_3^-$, which somewhat reduced Cs^+ adsorption capacity of ZrP-PS. However, different radius and dehydration enthalpy of hydrated Cs^+ and competitive cations determine the approachability to α-ZrP interlayers for these cations. The dehydration enthalpy for alkali metal and alkali earth metal ions increases with hydration radius, in the order of Cs^+ (3.29 Å) < Na^+ (3.58 Å) < Ca^{2+} (4.12 Å) < Mg^{2+} (4.28 Å) [61–64]. This order indicates that it is more facile for hydrated Cs^+ to dehydrate than hydrated Na^+, Ca^{2+}, and Mg^{2+}. Cs^+ enter the interlayers of α-ZrP and exchange with protons, however, hydrated Na^+, Ca^{2+} and Mg^{2+} are too large to fit the interlayer channels. Therefore, Na^+, Ca^{2+} and Mg^{2+} demonstrate little competition onto the inter-

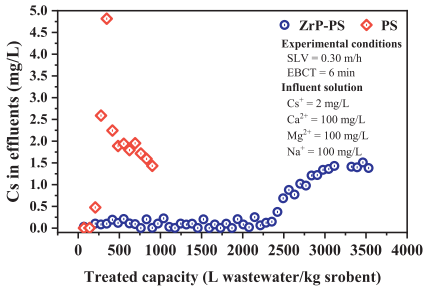

Fig. 4. Assessment of continuous sorption performances of ZrP-PS and PS (SLV: 0.3 m/h, EBCT: 6 min, Cs^+: 2 mg/L, Ca^{2+}: 100 mg/L, Mg^{2+}: 100 mg/L, Na^+: 100 mg/L).

layer proton exchange sites. Nanocrystalline and porous structures with particular channel or ring window sizes are also reported in other studies for selectively removing Cs^+ or Sr^{2+} from aqueous solutions [19,20,65]. In all, the synergy of size-screen assisted ion exchange of confined α-ZrP and -SO_3^- preconcentration of PS contributes to the efficient sequestration of cesium.

The practicality of ZrP-PS for cesium sequestration was evaluated by a simulated emergency treatment test using flow-through columns packed with ZrP-PS and PS, respectively, with the results shown in Fig. 4. As expected, ZrP-PS demonstrated a considerable improvement in Cs^+ removal efficiency over PS. After a continuous run of approximately 2300 liters per kilo sorbents, Cs^+ concentration in the effluent from the ZrP-PS column rose, reaching the breakthrough at ~3200 liters per kilo sorbents. In contrast, the effluent was only approximately 208 liters per kilo sorbents at the breakthrough of PS. It is noteworthy that for PS, the concentration of Cs^+ in the effluent around 300 L/kg sorbent was higher than 2 mg/L, which can be explained by the elution effect in continuous sorption [66,67]. Some Cs^+ initially sorbed by PS was replaced by competing cations Na^+, Ca^{2+}, and Mg^{2+} because of the nonspecific effect of -SO_3^- on these cations. Due to the specific affinity of α-ZrP for Cs^+, the elution effect in Cs^+ adsorption by ZrP-PS was suppressed, and therefore a larger treatment capacity was obtained. The amount of water treated by ZrP-PS was more than ten times that of PS, indicating the promising application of PS-confined α-ZrP nanocrystalline.

In summary, we developed efficient cesium sequestration using the PS confined α-ZrP nanocrystalline. Macropores and -SO_3^- in the PS host permitted uniform dispersion of α-ZrP, whose interlayer spacing screened competitive hydrated cations out and allowed Cs^+ retention on interlayer ion exchange sites. The specific ion exchange and nonspecific electrostatic reaction synergistically prompted a high Cs^+ adsorption capacity of 269.58 mg/g and a quick equilibrium within 80 min. The continuous treatment exhibited a remarkable capacity of approximately 2300 L water/kg ZrP-PS. Given its efficient cesium sequestration and flexibility to separate from treated water, ZrP-PS has excellent potential for emergency treatment and deep purification of radioactively contaminated water.

Declaration of competing interest

The authors declare that they have no known competing financial interests or personal relationships that could have appeared to influence the work reported in this paper.

Acknowledgments

This work was financially supported by NSFC (Nos. U22A20403, 21301151 and 52070115), Natural Science Foundation of Hebei Province (Nos. B2021203036 and E2022203011), and Key Project of the Hebei Education Department (No. ZD2021103).

Supplementary materials

Supplementary material associated with this article can be found, in the online version, at doi:10.1016/j.cclet.2023.108442.

References

[1] K. Matsuda, S. Yamamoto, K. Miyamoto, J. Environ. Radioact. 222 (2020) 106350.
[2] E. Lyman, M. Schoeppner, F.V. Hippel, Science 356 (2017) 808–809.
[3] P.C. Burns, R.C. Ewing, A. Navrotsky, Science 335 (2012) 1184–1188.
[4] P.P. Povinec, M. Gera, K. Holy, et al., Appl. Radiat. Isot. 81 (2013) 383–392.
[5] S. Khandaker, Y. Toyohara, G.C. Saha, M.R. Awual, T. Kuba, J. Water Process Eng. 33 (2020) 101055.
[6] B. Ma, S. Oh, W.S. Shin, S.J. Choi, Desalination 276 (2011) 336–346.
[7] C. Rouas, H. Bensoussan, D. Suhard, et al., Chem. Res. Toxicol. 23 (2010) 1883–1889.
[8] S. Chen, J. Hu, S. Han, et al., Sep. Purif. Technol. 251 (2020) 117340.
[9] S. Kwon, J. Choi, S. Cho, et al., J. Radioanal. Nucl. Chem. 311 (2016) 1605–1611.
[10] L. Zhu, X. Hou, J. Qiao, Talanta 221 (2021) 121637.
[11] Y.M. Zhao, M. Sun, L. Cheng, et al., J. Hazard. Mater. 425 (2022) 128007.
[12] X. Liu, Z. Lei, X. Zhao, J. Radioanal. Nucl. Chem. 331 (2022) 5709–5717.
[13] E. Tokar, M. Tutov, S. Bratskaya, A. Egorin, Molecules 27 (2022) 8937.
[14] J. Wang, S. Zhuang, Rev. Environ. Sci. Biotechnol. 18 (2019) 231–269.
[15] Z. Chen, W. Wei, H. Chen, B.J. Ni, Eco Environ. Health 1 (2022) 86–104.
[16] S. Rengaraj, K.H. Yeon, S.Y. Kang, et al., J. Hazard. Mater. 92 (2002) 185–198.
[17] W. Zhu, X. Huang, Y. Zhang, et al., Chin. Chem. Lett. 32 (2021) 3382–3386.
[18] B.R. Figueiredo, S.P. Cardoso, I. Portugal, J. Rocha, C.M. Silva, Sep. Purif. Rev. 47 (2018) 306–336.
[19] J. Zhang, L. Chen, X. Dai, et al., Chem. Commun. 57 (2021) 8452–8455.
[20] J. Zhang, L. Chen, X. Dai, et al., Chem 5 (2019) 977–994.
[21] T. Yuan, Q. Chen, X. Shen, Chin. Chem. Lett. 31 (2020) 2835–2838.
[22] Q. Zhang, S. Bolisetty, Y. Cao, et al., Angew. Chem. Int. Ed. 58 (2019) 6012–6016.
[23] Q. Wang, D. Yu, Y. Wang, J. Sun, J. Shen, Langmuir 24 (2008) 11684–11690.
[24] A. Clearfield, J.A. Stynes, J. Inorg. Nucl. Chem. 26 (1964) 117–129.
[25] Z. Ye, L. Chen, H. Chen, et al., Chem. Phys. Lett. 709 (2018) 96–102.
[26] W. Mu, Q. Yu, B. Chen, et al., J. Mol. Liq. 323 (2021) 114585.
[27] E. Chmielewská, J. Majzlan, M. Bujdoš, J. Radioanal, Nucl. Chem. 331 (2022) 3495–3504.
[28] Q. Zhang, P. Jiang, B. Pan, W. Zhang, L. Lv, Ind. Eng. Chem. Res. 48 (2009) 4495–4499.
[29] Q. Zhang, Q. Du, T. Jiao, et al., Chem. Eng. J. 221 (2013) 315–321.
[30] Q. Zhang, Q. Du, T. Jiao, et al., Sci. Rep. 3 (2013) 2551.
[31] Q. Sun, Y. Yang, Z. Zhao, et al., Environ. Sci. Nano 5 (2018) 2440–2451.
[32] D. Asante-Sackey, S. Rathilal, E. Kweinor Tetteh, E.O. Ezugbe, L.V. Pillay, Membranes 11 (2021) 128–132.
[33] X. Zhang, P. Huang, S. Zhu, M. Hua, B. Pan, Environ. Sci. Technol. 53 (2019) 5319–5327.
[34] B. Pan, B. Pan, X. Chen, et al., Water Res. 40 (2006) 2938–2946.
[35] S. Pan, J. Shen, Z. Deng, X. Zhang, B. Pan, J. Hazard. Mater. 423 (2022) 127158.
[36] Y. Cheng, X.D. Wang, S. Jaenicke, G.K. Chuah, Inorg. Chem. 57 (2018) 4370–4378.
[37] A. Clearfield, W.L. Duax, A.S. Medina, G.D. Smith, J.R. Thomas, J. Phys. Chem. C 73 (1969) 3424–3430.
[38] A. Clearfield, G.D. Smith, Inorg. Chem. 8 (1969) 431–436.
[39] G. Alberti, R. Vivani, F. Marmottini, P. Zappelli, J. Porous Mater. 5 (1998) 205–220.
[40] H. Benhamza, P. Barboux, A. Bouhaouss, F.A. Josien, J. Livage, J. Mater. Chem. 1 (1991) 681–684.
[41] X. Zhang, J. Shen, S. Pan, J. Qian, B. Pan, Adv. Funct. Mater. 30 (2020) 1909014.
[42] P. Jiang, B. Pan, B. Pan, W. Zhang, Q. Zhang, Colloid. Surface A 322 (2008) 108–112.
[43] G. Alberti, M.G. Bernasconi, M. Casciola, U. Costantino, J. Chromatog. A 160 (1978) 109–115.
[44] A. Clearfield, G.A. Day, A. Ruvarac, S. Milonjic, J. Inorg, Nucl. Chem. 43 (1981) 165–169.
[45] J.H. Tang, J.C. Jin, W.A. Li, et al., Nat. Commun. 13 (2022) 658.
[46] Y. Seo, Y. Hwang, J. Environ. Chem. Eng. 9 (2021) 105950.
[47] T. Xia, L. Yin, Y. Xie, Y. Ji, Chem. Phys. Lett. 746 (2020) 137293.
[48] S. Chen, J. Hu, J. Shi, et al., J. Hazard. Mater. 371 (2019) 694–704.
[49] E. Han, Y.G. Kim, H.M. Yang, I.H. Yoon, M. Choi, Chem. Mater. 30 (2018) 5777–5785.
[50] M. Gou, Z. Yu, P. Na, J. Nucl. Radiochem. 39 (2017) 290–297.
[51] H. Deng, Y. Li, L. Wu, X. Ma, J. Hazard. Mater. 324 (2017) 348–356.
[52] Z. Majidnia, A. Idris, Chem. Eng. J. 262 (2015) 372–382.
[53] H. Yang, L. Sun, J. Zhai, et al., J. Mater. Chem. A 2 (2014) 326–332.
[54] D. Ding, Y. Zhao, S. Yang, et al., Water Res. 47 (2013) 2563–2571.
[55] G. Grzybek, P. Stelmachowski, S. Gudyka, et al., Appl. Catal. B: Environ. 168-169 (2015) 509–514.
[56] A. Clearfield, Mater. Chem. Phys. 35 (1993) 257–263.
[57] A.S. Singh, D.R. Naikwadi, K. Ravi, A.V. Biradar, Mol. Catal. 521 (2022) 112189.
[58] K. Wang, H. Ma, S. Pu, et al., J. Hazard. Mater. 362 (2019) 160–169.
[59] G. Alberti, U. Costantino, S. Allulli, M.A. Massucci, J. Inorg. Nucl. Chem. 37 (1975) 1779–1786.
[60] G. Alberti, Accounts Chem. Res. 11 (1978) 163–170.

[61] L. Catala, T. Mallah, Coordin. Chem. Rev. 346 (2017) 32–61.
[62] M. Yamada, M. Arai, M. Kurihara, M. Sakamoto, M. Miyake, J. Am. Chem. Soc. 126 (2004) 9482–9483.
[63] Y. Wu, J. Chen, Z. Liu, P. Na, Z. Zhang, J. Environ. Chem. Eng. 10 (2022) 108073.
[64] S. Uchida, Chem. Sci. 10 (2019) 7670–7679.
[65] Y. Wang, Z. Liu, Y. Li, et al., J. Am. Chem. Soc. 137 (2015) 6144–6147.
[66] Q. Zhang, B. Pan, B. Pan, et al., Environ. Sci. Technol. 42 (2008) 4140–4145.
[67] M. Wen, Z. Ma, D.B. Gingerich, X. Zhao, D. Zhao, Eco Environ. Health. 1 (2022) 219–228.